



Identifying priority air pollution management areas during the burning season in Nan Province, Northern Thailand

Daroonwan Kamthonkiat¹ · Juthasinee Thanyapraneedkul¹ ·
Nithima Nuengjumnong¹ · Sarawut Ninsawat² · Kessinee Unapumnuk³ ·
Tuong Thuy Vu⁴

Received: 28 August 2019 / Accepted: 1 July 2020 / Published online: 8 July 2020
© Springer Nature B.V. 2020

Abstract

In northern Thailand, biomass burning is a major source of high concentrations of particulate matter with a diameter $< 10 \mu\text{m}$ (PM_{10}) during the burning season (January to May), leading to health concerns related to air pollution. Given the limited staffing and budget available to local agencies, identifying priority areas for management and mitigation is important. We herein developed an empirical model using Landsat 8 imagery and PM_{10} data from ground stations to estimate PM_{10} concentrations in Nan Province, achieving an error of $< 20\%$ between the predicted and measured PM_{10} values. The satellite-derived values were then classified into five air quality levels based on criteria defined by the Thai Ministry of Natural Resources and Environment. These levels were correlated with land use/land cover maps and fire hotspots with high confidence ($> 80\%$) acquired by the Terra and Aqua satellites from January to May 2015–2019. Fire hotspots and problematic PM_{10} concentrations were most often correlated with agricultural land, followed by disturbed forests and dense forests. These results enabled us to identify critical areas where repeat burning and high PM_{10} levels should be prioritized for mitigation, such as the upland agricultural and forest areas of Wiang Sa District. Our methodology could benefit air pollution management in other developing countries with similar limitations.

Keywords Priority area analysis · PM_{10} concentration · Air pollution management · Biomass burning · Nan Province

1 Introduction

For more than a decade, the people of northern Thailand have suffered from air pollution caused by open agricultural burning and forest fires during dry and hot weather conditions from January to May, frequently called the fire season or burning season. During this time, local villagers set fires to burn rice straw or weeds in order to clear land, remove weeds, and

✉ Daroonwan Kamthonkiat
daroonwan.k@gmail.com

Extended author information available on the last page of the article

control disease before starting new crops. Forests and underbrush are also burned to enhance the reproduction and propagation of natural crops such as mushrooms or the edible plants *Sauropus androgynus* and *Melientha suavis*. These fires produce large amounts of small particulate matter (PM) in the northern provinces of Thailand (Chiang Rai, Chiang Mai, Mae Hong Son, Lampang, Lumphun, Phayao, Nan, Phrae, and Uttaradit). These aerosols are a serious threat to public health and tourism (Jeensorn et al. 2018; Silva et al. 2016; Air Quality and Noise Management Bureau of Thailand 2013; Ryan et al. 2013). However, the local staff and budget available to deal with air pollution management are limited in Thailand and most developing countries; thus, identifying and prioritizing critical areas (those experiencing repeated burning and unhealthy concentrations of PM₁₀, i.e., PM with a diameter < 10 µm) would be beneficial.

For many decades, satellite-based remote sensing has been a useful tool for mapping changes in land use/land cover (LULC). Furthermore, many remote sensing applications have been developed for retrieving aerosol optical depth (AOD) or aerosol optical thickness (AOT) air quality measurements using moderate- to low-resolution data from the MODerate-resolution Imaging SpectroRadiometer (MODIS) or Multi-angle Imaging SpectroRadiometer (MISR) aboard the Terra satellite or various Landsat products. The derived AOD/AOT or atmospheric reflectance can then be compared to PM_{2.5} (PM with a diameter < 2.5 µm) or PM₁₀ data acquired from other instruments such as the Aerosol Robotic Network (AERONET), physical measurements (such as sun photometers, spectroradiometers, and PM laser photometers), or local air quality measurement stations (Dumitrache et al. 2016; Meng et al. 2016; Hagolle et al. 2015; Benas et al. 2013; Bhaskaran et al. 2011; Othman et al. 2010; Hadjimitsis 2009). Remote sensing PM₁₀ data enable the estimation of air pollution levels over large and remote areas. AOD images from MODIS are widely used to develop PM_{2.5} and PM₁₀ estimation algorithms at global or regional scales, while Landsat images are more suitable for local or provincial studies (Roy et al. 2017; Saraswat et al. 2017; Shaheen et al. 2017; Saleh and Hasan 2014; Mishra et al. 2012). However, the AOD/AOT retrieval algorithm for PM estimation from Landsat is not as well developed as it is for MODIS (Sun et al. 2016; Glantz and Tesche 2012; Remer et al. 2005; von Hoyningen-Huene et al. 2003).

In this study, we used multi-temporal Landsat 8 imagery acquired during the 2015–2017 fire seasons in Nan Province, northern Thailand, to analyze PM₁₀ concentrations and land use. The estimated PM₁₀ concentrations were then classified to health risk levels based on criteria defined by Thailand's Air Quality and Noise Management Bureau, Pollution Control Department, Ministry of Natural Resources and Environment. Areas with high PM₁₀ levels were also correlated with LULC type (Vadrevu et al. 2018; Zahari et al. 2016; Zou et al. 2016b; Wu et al. 2012), and the locations of biomass burning or fires (hotspot data from the MODIS sensor) acquired during the 2015–2019 fire seasons. This enabled identifying and prioritizing critical areas experiencing repeated burning and unhealthy PM₁₀ levels for improved air pollution management. These findings will be useful for many local agencies tasked with air pollution control, fire management, forest conservation, disaster prevention and mitigation, public health, and land use or agricultural planning. Such agencies can use the resulting data as a resource for deciding where to focus local efforts and for developing strategic plans for air pollution management.

2 Materials and methods

2.1 Study area

Nan Province is bordered by many mountainous forested national parks, with a narrow swath of flat terrain in the middle of the province. Almost 900 villages are located in 99 sub-districts (Tambon) within 15 districts (Amphoe). Most villagers work in the agricultural sector growing maize, rice, rubber, tree fruits (longan, mango, lychee, tamarind, lambutan, etc.), teak, and other crops. Agricultural land use in Nan has increased for at least the past decade, making biomass burning an increasingly critical issue in this area (Nan Statistical Office Annual Report 2015–17). Figure 1 presents a map of the study area showing the provincial boundary of Nan (highlighted boundary) and neighboring provinces where eight of the PM₁₀ monitoring stations used in this study were located (all in the same Landsat scene; path–row 130–47) as well as the main roads in Nan. In addition, the industrial land consisted of agricultural product (dry longan, tobacco, rice mill) and teak processing plant in Nan was overlaid. Small-scale or household industrial land uses cover less than 2% of the entire areas in Nan; hence, these small portions cannot be seen clearly on the map. These components were overlaid on the mosaicked scenes from Landsat 8 (Path–Row: 129–47, 130–46, and 130–47) acquired in 2015.

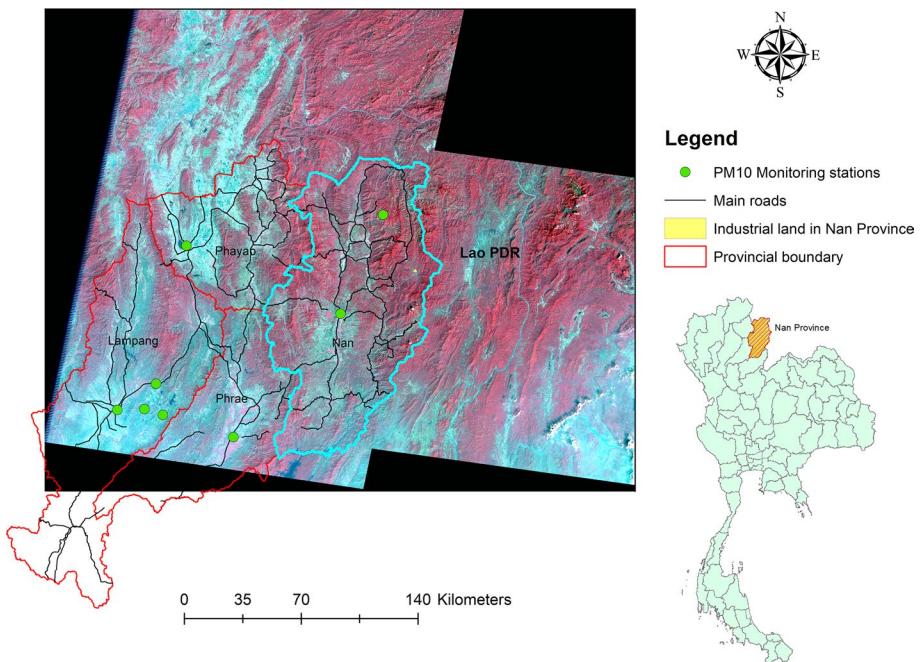


Fig. 1 Study area

2.2 Data

The details of all imagery, air quality data, and other data used in this study are given in Table 1. We used three Landsat 8 scenes to cover all of Nan, as 70% of the area was within Path–Row 130–47, as well as most ground stations (see Fig. 1). In addition, cloud-free images are rare in Southeast Asia or the tropical climate zone; thus, some cloudy or smoky scenes were initially included. After defining the PM_{10} concentration maps, images that had high error levels were omitted to avoid overestimating unhealthy areas (Table 2). Unfortunately, most of the Landsat 8 operational land imager (OLI) images acquired during January–May 2018 had serious cloud contamination problems; therefore, we could not produce PM_{10} concentration maps for 2018.

Thailand has a limited number of AERONET member stations, the closest of which is located in Chiang Mai Province, almost 300 km from Nan (NASA 2018). Therefore, in situ PM_{10} time series data were collected from eight Thai Pollution Control Department air quality measurement stations located in Nan and neighboring provinces (see Fig. 1). A few meteorological stations are located in Muang Nan (almost 10 km from the PM_{10} monitoring station located in the central of Muang Nan), Tha Wang Pha, and Thung Chang. However, the observations in these stations have limited parameters and are aimed at agricultural activities. Because of the uncomplete historical data and less significant weather fluctuations during our observed period, the burning season (dry weather), these meteorological parameters were not included in our analysis.

2.3 Methods

The study methodology is presented in Fig. 2. First, the selected Landsat data were processed for radiometric calibration by converting the digital number (DN) of the multi-spectral OLI data (using no thermal bands; Table 3) to the top-of-atmosphere (TOA) radiance using the radiance rescaling factors in the Landsat metadata (MTL) file as follows (Vermote et al. 2016):

$$L_{\lambda} = M_L \times Q_{\text{cal}} + A_L \quad (1)$$

where L_{λ} is the TOA spectral radiance ($W m^{-2} sr^{-1} \mu m^{-1}$), M_L is the band-specific multiplicative rescaling factor from the metadata (Radiance_Mult_Band_x, where x is the band number), A_L is the band-specific additive rescaling factor from the metadata (Radiance_Add_Band_x), and Q_{cal} is the quantized and calibrated standard product pixel values (DN).

The multi-spectral radiance images were then processed for atmospheric correction using the Fast Line-of-sight Atmospheric Analysis of Hypercubes (FLAASH) algorithm in the Environment for Visualizing Images (ENVI) application (Exelis Visual Information Solutions, Inc. 2013). FLAASH incorporates the MODerate-resolution atmospheric TRANsmission (MODTRAN) radiation transfer code and works well with wavelengths from those in the visible light range up to 3 μm . Each image was computed based on the specific standard MODTRAN model atmospheres and aerosol types, with surface reflectance (SR) bands as the output:

$$L = \frac{A\rho}{1 - \rho_e S} + \frac{B\rho_e}{1 - \rho_e S} + L_a \quad (2)$$

Table 1 Data sources

No.	Data	Source
1	Landsat 8—operational land imager (OLI), (path—row: 129–47, 130–46 and 130–47) acquired during 2015–2017	US Geological Survey (USGS)
2	Air quality measurement stations and PM ₁₀ data (hourly) during 2015–2017	Air Quality and Noise Management Bureau
3	Digital maps (scale 1:50,000); Administrations boundaries, roads, villages	Ministry of Interior
4	Hotspots from Terra/Aqua (2015–2019 during fire season or from Jan. to May)	Fire Information for Resource Management System (FIRMS), NASA and Department of National Parks, Wildlife and Plant Conservation, the Ministry of Natural Resources and Environment

Table 2 Specific Landsat 8 scenes used

Month	2015 (path–row)		2016 (path–row)		2017 (path–row)	
	(129–47)	(130–46)	(129–47)	(130–46)	(129–47)	(130–46)
January	20150120	20150127	–	–	20170125	20170116
February	20150221	20150228	20160208	20160215	20170210	20170201, 20170217
March	20150309	20150316	20160311	20160318	20170314, 20170330	20170305, 20170321
April	20150426	20150401	20160412	20160403	20170415	20170422
May	–	–	20160514	20160505	–	–

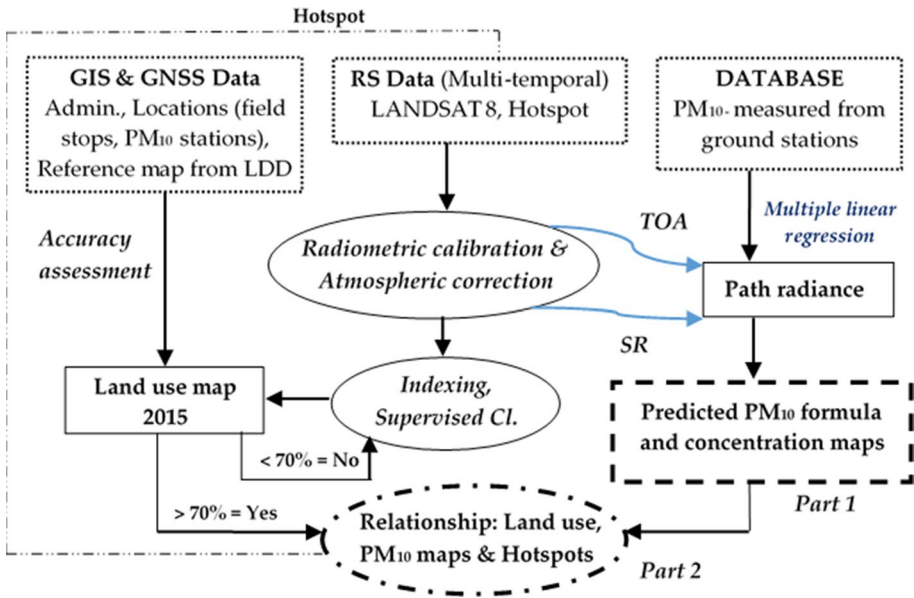


Fig. 2 Methodology flowchart

Table 3 Landsat 8 OLI bands used in this study

Band	Wavelength (μm)	Spatial resolution (m)	Independent variables (Eqs. 3 and 4)
Band 1 ultra blue (coastal/aerosol)	0.435–0.451	30	X1
Band 2 blue	0.452–0.512	30	X2
Band 3 green	0.533–0.590	30	X3
Band 4 red	0.636–0.673	30	X4
Band 5 near infrared (NIR)	0.851–0.879	30	X5
Band 6 shortwave infrared 1 (SWIR 1)	1.566–1.651	30	X6
Band 7 shortwave infrared 2 (SWIR 2)	2.107–2.294	30	X7

where ρ is the pixel SR, ρ_e is an average SR for the pixel and surrounding region, S is the spherical albedo of the atmosphere, L_a is the radiance backscattered by the atmosphere, and A and B are coefficients that depend on atmospheric and geometric conditions, respectively, but not at the surface.

The difference between the derived TOA and SR is the path radiance (PR), which represents noise or radiance that is backscattered by particles and molecules in the atmosphere. Therefore, it was used to estimate the PM₁₀ concentration in the air (Fernández-Pacheco et al. 2018; Roy et al. 2017; Yoram 1993). The PR images were correlated with PM₁₀ (μg m⁻³) acquired on the same date and time at the air quality measurement stations. The correlation between each PR image (independent parameter) and PM₁₀ from the stations (dependent parameter) when compared at the same geographic location was calculated as follows:

$$Y = aX + b \quad (3)$$

where a is the gradient slope, b is the y intercept, and X is the variable. The R^2 of each band in each PR image varied from less than 0.1 to 0.86. We selected only the linear regression equations from bands/dates with high correlations ($R^2 \sim 0.7$ or higher) to further estimate PM_{10} , such as the correlation between Band 1 (X1 or PR derived from the Band 1/ultra blue (coastal/aerosol)) acquired on February 28, 2015, and the PM_{10} values measured at ground stations on the same date. The linear regression with the highest R^2 (0.85,885) was used for PM_{10} prediction; the following derived linear Eq. (4) was applied to the image for PM_{10} estimation:

$$Y = 0.00004X + 0.01224 \quad (4)$$

However, higher correlation coefficients were found for different bands on different dates. Thus, the relationship between several independent parameters or bands of PR images (multi-spectral and multi-temporal) and PM_{10} values measured from ground stations in the study area (dependent parameters) was analyzed using a multiple linear regression equation:

$$Y' = a_0 + a_1X1 + a_2X2 + \dots + a_nXn \quad (5)$$

where Y' is the predicted PM_{10} (dependent variable), $X1$ through Xn are predictor variables (Table 3), a_0 is the value of Y' when all independent variables are equal to zero, and a_1 through a_n are the estimated regression coefficients. The best subset for use in the forecasting model for estimating PM_{10} was analyzed using the stepwise method that either began with *no* variables in the model and added one variable at a time (called *forward regression*) or began with *all* potential variables in the model and removed one variable at a time (called *backward regression*). In this study, the best subset of variables used in the forecasting model for the estimated PM_{10} comprised $X1$, $X4$, and $X7$, which had $R^2 = 0.704$ (RMSE $\sim 17 \mu\text{g m}^{-3}$).

The derived linear regression equations were applied to PR image(s) to predict PM_{10} values, which were compared to the PM_{10} measured at ground stations. The differences between the predicted and measured PM_{10} values were converted to percentages. Our predicted PM_{10} values showed less than 20% error and were then reclassified into five health impact levels (Table 4) based on guidelines from Thailand's Air Quality and

Table 4 Air quality classifications by PM_{10} level, based on Thai government standards

PM_{10} (24 h) $\mu\text{g}/\text{m}^3$	Air pollution level	Health implications
0–40	Good	Air quality is considered satisfactory, no risk
41–120	Moderate	Air quality is acceptable. There may be minor to moderate health concerns for a small number of people who are unusually sensitive to air pollution
121–350	Unhealthy	Most people may begin to experience health effects; members of sensitive groups (small children, the elderly, and those unusually sensitive to air pollution) may experience more serious health effects
351–420	Very unhealthy	The entire population is likely to experience health effects
> 420	Hazardous	Health alert: the entire population will experience serious health effects

Noise Management Bureau (2013), which in turn refer to US Environmental Protection Agency (1999) guidelines.

PM₁₀ data were consolidated by level and overlaid with LULC data derived from Landsat 8 imagery from January 27, 2015. The study area contained five main LULC classes: agricultural land (paddy fields, orchards, and crops), which covered 61.90% of Nan Province, dense forests (thickly treed and difficult to access by road) covered 14.75%, disturbed forests (treed but mostly disturbed or accessed by human activities) covered 19.03%, developed land and other (construction and areas not matching the other classes) covered 3.99%, and water bodies covered 0.33% of the entire province. For each main class, we homogeneously defined sub-classes for supervised maximum-likelihood classification. The classification results were validated using ground-truth data from 2015, while the forest status was rechecked using field data from 2016 and 2017. Table 5 presents the accuracy and error percentages (error of omission and commission) of each LULC class in the confusion matrix. Every class exceeded the expected 70% accuracy, although disturbed forests (accuracy = 78.85%) were confused with agricultural land (error of omission = 10.38%, error of commission = 13.46%) and dense forests (error of omission = 12.90% and error of commission = 7.69%). The accuracy of the classified images was high (overall accuracy = 85.42%, Kappa coefficient = 79.85%); thus, they were used for a correlation analysis in the next step.

The active fire hotspot data represent geographic coordinates with strong emissions in the mid-infrared (4 μm and 11 μm) wavelengths, as detected by the MODIS sensor on the Terra satellite in the morning and on the Aqua satellite in the afternoon. However, some pixels had higher temperatures than surrounding pixels, although no fire was present (these so-called “artificial fires” included metal roofs or other areas that appear to be very bright). The confidence of fire occurrence should therefore be considered when using this product (Junpen et al. 2013). We selected hotspot data during 2015–2019 with > 80% confidence values, and we correlated these real fire pixels with the LULC and PM₁₀ concentration maps. The occurrence of more frequent fires and unhealthy PM₁₀ concentrations implied more critical environmental problems (fires and air pollution) in an area and represented problematic human practices such as slash-and-burn techniques (converting forests to agricultural lands, burning fields before starting new

Table 5 Accuracy assessment of the LULC 2015 in Nan Province classified from Landsat 8 OLI

Class	Agricultural land (%)	Developed/other (%)	Dense forests (%)	Disturbed forests (%)	Water bodies (%)	Total area for validation (%)
Agricultural land	84.91	10.00	3.23	13.46	0.00	42.08
Developed/other	3.77	90.00	0.00	0.00	0.00	12.92
Dense forests	0.94	0.00	83.87	7.69	0.00	12.92
Disturbed forests	10.38	0.00	12.90	78.85	0.00	23.33
Water bodies	0.00	0.00	0.00	0.00	100.00	8.75
Total % of class accuracy and errors	100.00	100.00	100.00	100.00	100.00	100.00

crops) and adverse health impacts on local residents. Finally, critical areas were identified for management prioritization at the district level.

3 Results

3.1 PM₁₀ concentrations

Only six PM₁₀ images with $\leq 20\%$ error were classified by air quality (Fig. 3); the area of each classification is summarized in Table 6. In January 2015, good air quality (9566 km²; $\sim 78\%$) occurred over most of the study area, especially in mountainous areas, while moderate air quality (2638 km²; $\sim 22\%$) was found in the lower central region of the province. In February 2015, unhealthy (2854 km²; $\sim 23\%$) and very unhealthy (902 km²; $\sim 7\%$) air qualities were centered in southern mountainous areas including the Wiang Sa, Na Noi, and Na Muen districts, caused by southerly dry season flow and increased burning. In March 2015, unhealthy air quality (11,230 km²; $\sim 92\%$) dominated the province along with areas of very unhealthy air quality (974 km²; $\sim 8\%$). In February 2016, moderate air quality (9798 km²; $\sim 80\%$) was dominant, with unhealthy air quality (2406 km²; $\sim 20\%$) occurring in some central and mountainous western regions including the Wiang Sa, Na Noi, Na Muen, and Mueang Nan districts. In February 2017, good (8799 km²; $\sim 72\%$) and moderate (3406 km²; $\sim 28\%$) air qualities dominated. In March 2017, unhealthy (7223 km²; $\sim 59\%$) and very unhealthy (2379 km²; $\sim 19\%$) air qualities were most common, including in the Wiang Sa, Na Noi, Mae Charim, Mueang Nan, and Na Muen districts. Unhealthy and very unhealthy air qualities were predominant in Wiang Sa District for all dates, followed by the Na Noi district.

3.2 Relationship between PM₁₀ concentrations, LULC, and hotspots

We selected areas classified as unhealthy and very unhealthy during February 2015, March 2015, February 2016, and March 2017 and calculated their overlays with LULC types (Table 7). It was found that $> 60\%$ of unhealthy and very unhealthy areas in the observed periods were related to agricultural land, $< 20\%$ to forest, and $< 4\%$ to other classes.

During the 2015–2019 burning seasons, 1515 hotspots were identified in the study area (695, 294, 147, 118, and 297 in 2015, 2016, 2017, 2018, and 2019, respectively). Only $\sim 1\text{--}2\%$ of the total hotspots were observed in January or February, but this percentage increased drastically in March (in 2015–2019, $\sim 42\%$, $\sim 22\%$, $\sim 40\%$, $\sim 30\%$, and $\sim 31\%$, respectively). The largest number of hotspots was observed in April ($\sim 56\%$, $\sim 69\%$, $\sim 48\%$, $\sim 52\%$, and $\sim 26\%$ in 2015, 2016, 2017, 2018, and 2019, respectively), but their occurrence fell significantly in May ($\sim 0\%$, $\sim 5\%$, $\sim 9\%$, $\sim 2\%$, and $\sim 10\%$ in 2015, 2016, 2017, 2018, and 2019, respectively). Overall, $\sim 67\%$ of the total hotspots occurred over agricultural land, $\sim 16\%$ over disturbed forest, $\sim 13\%$ over dense forest, and $\sim 2\%$ over developed land (Table 8). In 2015, the largest number of hotspots occurred on agricultural lands ($\sim 91\%$) and forest areas ($\sim 5\%$ in disturbed forest and $\sim 2\%$ in dense forest) in the Wiang Sa, Chaloeam Phra Kiat, Bo Kluea, Pua, Na Noi, Na Muen, Thung Chang, and Mae Charim districts, with similar patterns in 2016 and 2017, although with lower overall totals (Fig. 4). In 2018 and 2019, the largest number of hotspots occurred followed a similar pattern as that in 2015 to 2017 on agricultural lands ($\sim 64\%$) and forest areas ($\sim 16\%$ in disturbed forest and $\sim 16\%$ in dense forest). The number of hotspots in 2019 was close to the

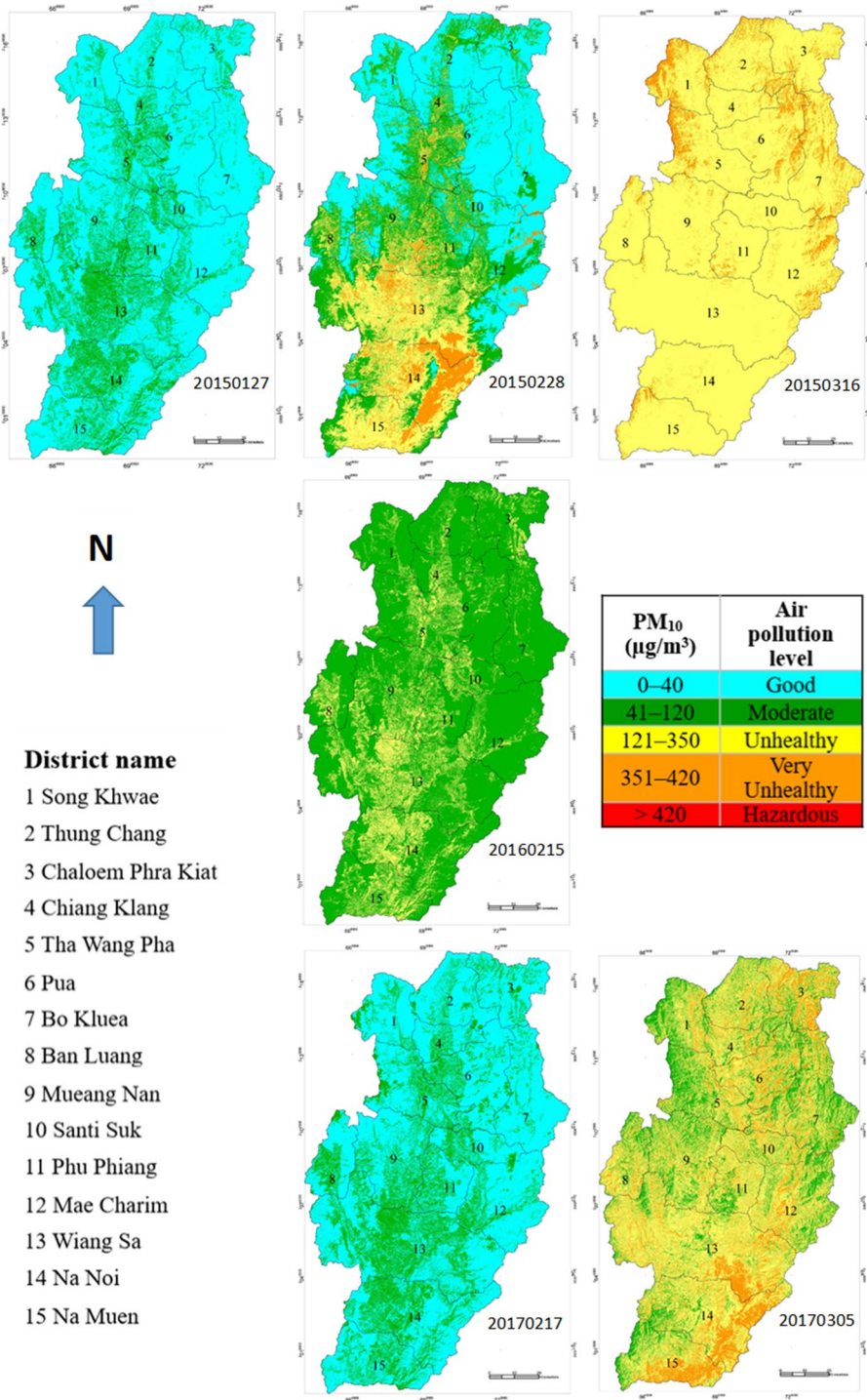


Fig. 3 Monthly air quality maps during the 2015–2017 burning seasons in Nan Province, Thailand

Table 6 Spatial coverage (%) of air quality levels on certain days (see Fig. 3) during the burning seasons in Nan Province, Thailand

PM ₁₀ ($\mu\text{g m}^{-3}$)	Air pollution level	Landsat Image Acquisition Dates (see Fig. 3)					
		Jan. 27, 2015	Feb. 28, 2015	Mar. 16, 2015	Feb. 15, 2016	Feb. 17, 2017	Mar. 5, 2017
0–40	Good	78.38	40.87	0	0	72.09	0.00
41–120	Moderate	21.62	28.35	0	80.28	27.91	21.32
121–350	Unhealthy	0	23.39	92.02	19.72	0	59.18
351–420	Very unhealthy	0	7.39	7.98	0	0	19.49
>420	Hazardous	0	0	0	0	0	0.00
Total		100	100	100	100	100	100

Table 7 Correlation between unhealthy and very unhealthy air quality levels and LULC types by observation

LULC type	February 28, 2015		March 16, 2015		February 15, 2016		March 5, 2017	
	km ²	%	km ²	%	km ²	%	km ²	%
Water	24.76	0.66	39.78	0.33	1.89	0.08	31.78	0.38
Dense forest	29.76	0.79	1799.83	14.75	0.84	0.04	1656.03	19.76
Disturbed forest	401.73	10.70	2323.14	19.04	56.26	2.34	1181.02	14.09
Developed/other	101.41	2.70	486.60	3.99	240.69	10.00	328.10	3.91
Agriculture	3198.39	85.15	7555.13	61.90	2106.73	87.55	5185.53	61.86
Sum	3756.05	100	12,204.48	100	2406.41	100	8382.46	100.00
% of study area	30.78		100		19.72		68.68	

Table 8 Number of hotspots observed during the burning season by LULC category

LULC type	2015	2016	2017	2018	2019	Total
Dense forest	85	49	32	20	45	231
Disturbed forest	109	43	29	19	48	248
Developed/others	14	10	4	3	11	42
Water	3	0	1	0	1	5
Agricultural land	448	192	81	76	192	989
Total	659	294	147	118	297	1515

number that occurred in 2016, which was higher than the number in 2017 and 2018, while more hotspots were distributed in agricultural land and forest areas than in the previous years. Overall, Wiang Sa had the most fires, followed by the Pua, Na Noi, and Chaloe Phra Kiat districts.

Unhealthy and very unhealthy PM₁₀ concentrations began to cover the southern and central parts of the study area in February, especially in the Wiang Sa, Na Noi, Mae Charim, Mueang Nan, and Na Muen districts. This expanded to the entire study area in March

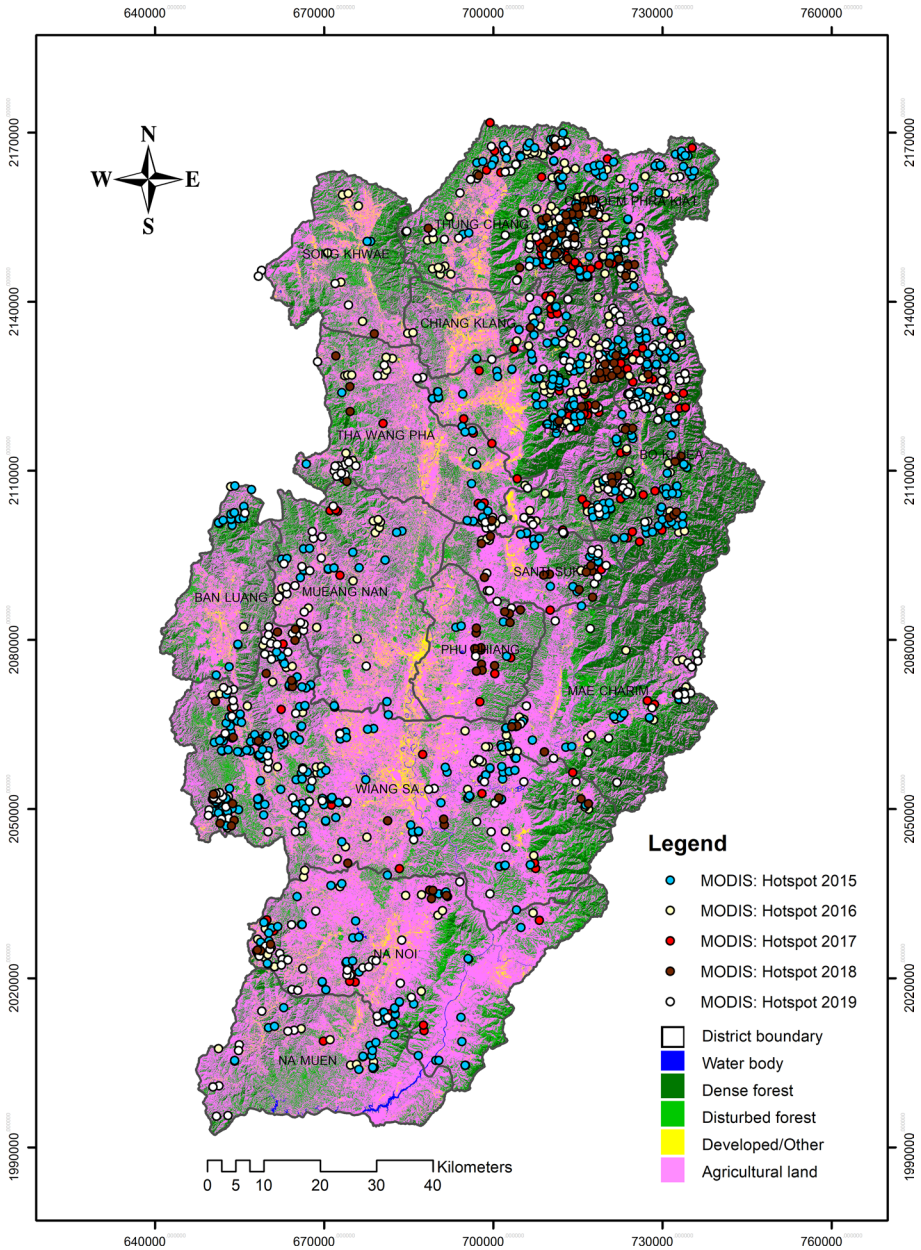


Fig. 4 2015 LULC classifications and MODIS-derived fire hotspots during 2015–2019 in Nan Province, Thailand

due to southerly winds and new burning sites (Thai Meteorological Department 2015). Burning hotspots reoccurred most commonly on agricultural lands in the central and northern parts of Nan Province. Although hotspots in disturbed and dense forests were much less common, they ranked second and third in terms of reoccurrence.

Based on information from Thailand's Air Quality and Noise Management Bureau, biomass burning and unhealthy PM_{10} both peak in March every year. During this time, Wiang Sa and Na Noi were the most critical districts for air pollution according to the results of our study. Several villages in the Wiang Sa District, namely Naka Village in the Yai Hua Na Sub-district and Wana Prai and Nam Pi villages in the Nam Muab Sub-district, were located near highly repetitive burn sites and should be prioritized for air pollution management by collaborating with local villagers. Specifically, villagers should be encouraged to adjust their practices and behavior by stopping open burning, creating fire barriers (open buffer zones between forest and other land uses), preserving forests, monitoring and reporting fires to the appropriate agency, and taking greater personal care for their health during unhealthy air pollution conditions, among other measures.

4 Discussion

In this study, the correlation between three PR images calculated from the coastal aerosol, red, and SWIR2 bands of Landsat 8 and ground station-based PM_{10} levels presented the highest correlation and lowest error. By contrast, Saleh and Hasan (2014) showed that the coastal aerosol, blue, and green bands of Landsat 8 showed the highest correlation and lowest error. The difference between our predicted and measured PM_{10} values was $<20\%$, which was acceptable for determining PM_{10} concentrations in different LULC types. However, our algorithm should be further developed in order to reduce errors that were mainly caused by the limited availability of cloud-free images and ground measurement data. Kanniah et al. (2016) suggested integrating aerosol products from various satellite sensors to overcome the cloudiness (a common phenomenon in Southeast Asia) and orbital gaps of satellite tracks. In many studies, meteorological parameters (atmospheric pressure, relative humidity, air temperature, wind direction and speed, etc.) have provided valuable support for enhancing the prediction of seasonal PM concentrations and dispersion patterns at the regional scale when they are incorporated with daily AQI data (which have high temporal resolution/high frequency) and AOD (high temporal resolution/high frequency but low spatial resolution) from satellites. Nonetheless, the prediction results have shown very random affects (Diao et al. 2019; Qiao et al. 2019; Kliengchuay et al. 2018; Kamarul Zaman et al. 2017; Chu et al. 2016; Yin et al. 2016). These parameters less effectively enhance PM_{10} prediction when low-temporal-resolution data or long gap satellite observations (medium to high spatial resolution) are incorporated at the local scale when the relative magnitude of meteorological parameters seem to be similar. In our case, not only were limited parameters recorded from the meteorological station in Nan Province, but also, we focused on PM_{10} concentration only in the burning season (January to May), which is a period of dry weather. Therefore, these meteorological parameters were not incorporated into our analysis. Land use information has also been mentioned in some reports as a necessary parameter for improving the reliability of predicting PM_{10} concentrations over different LULC or for different sources of pollution (Meng et al. 2016; Zahari et al. 2016; Zou et al. 2016b). In addition, in most of the previous studies, PM_{10} comes from incomplete combustion, automobile emissions, or dust from big cities, industrial areas, coalmines, and arid areas. By contrast, the major source of PM_{10} in this study was evidently biomass burning in forest areas and agricultural lands, and the locations of these fires and sources of PM_{10} were random or could not be fixed). Although LULC was not combined into our prediction model,

it was incorporated into the PM₁₀ concentration maps and hotspots in our analysis for identifying priority air pollution management areas.

More advance and complex models (nonlinear regression methods) have been developed for predicting PM (both PM_{2.5} and PM₁₀) using relevant covariates including high-temporal-resolution (e.g., daily) AOD products, meteorological parameters, land use information, or any related auxiliary data. For example, generalized additive model (GAM), which is an extension of multiple linear regression models, linear mixed-effects (LME) or mixed-effect model (MEM), geographically weighted regression (GWR), geographically and temporally weighted regression (GTWR), artificial neural network (ANN), support vector regression (SVR), and random forest (RF) have all been applied. Many studies compared the ability of the resulting developed models with the simple and widely used linear regression (Park et al. 2019; Li et al. 2018; Abdullah et al. 2019; Guo et al. 2017; Jiang et al. 2017; Zou et al. 2017; Kamarul Zaman et al. 2017; Chu et al. 2016; Nguyen et al. 2014). These additive or newly developed nonlinear models have presented higher correlation than linear regression when dealing with long-term and high-frequency data such as AOD/PM from satellites and ground-based PM observation data, daily meteorological parameters, LULC or source of pollution, and other related data. However, it has been difficult to conclude which prediction model is the best as their results have shown medium to high accuracies for large areas or at the national scale. However, many works have found that the linear regression method could still be used to predict PM concentrations, especially when only two parameters were considered, PM data from satellites (i.e., AOD, PR) and ground measurements. PM₁₀ concentrations have been found to increase linearly with the increase in PR or AOD, and the prediction results from the simple linear method presented medium to high accuracy (Roy et al. 2017; Shaheen et al. 2017; Nguyen et al. 2015; Glantz and Tesche 2012; Mishra et al. 2012; Themistocleous et al. 2012; Othman, et al. 2010). Our multi-spectral model accurately (high R^2) predicted PM₁₀ concentrations in the study area ($R^2=0.704$, RMSE $\sim 17 \mu\text{g m}^{-3}$). In addition, our model shows a similar accuracy to the one derived using nonlinear methods in previous studies that used the same number of or more input parameters ($R^2=0.3\text{--}0.99$, RMSE $=8\text{--}31 \mu\text{g m}^{-3}$).

Classifying the estimated PM₁₀ concentrations into the five classes defined by the Thai government (and based on US EPA guidelines), we showed that agricultural land, disturbed forest, and dense forest were repeatedly subjected to unhealthy levels of PM₁₀ concentrations ($> 120 \mu\text{g/m}^{-3}$) during the burning seasons of 2015–2017. Using different guidelines, Roy et al. (2017) found that approximately half of Vadodara city and Nandesari town in India showed unhealthy levels of PM₁₀ concentrations ($120\text{--}160 \mu\text{g/m}^{-3}$, with some small areas at $160\text{--}200 \mu\text{g/m}^{-3}$). However, they did not consider specific LULC types or extents. In the Gaza Strip, Shaheen et al. (2017) used two major land classes (urban and non-urban) to assess pollution levels at $28\text{--}144 \mu\text{g/m}^{-3}$. Most of their study area had good to moderate air quality. However, it is difficult to compare our results to those of studies that are presented for AOT or PM₁₀ concentrations in graduated colors and values (not in $\mu\text{g/m}^{-3}$), such as those reported by Themistocleous et al. (2012).

Although many studies have estimated PM₁₀ concentrations using satellite data (such as Landsat 8), to the best of our knowledge, this is the first time fire hotspots and LULC types have been integrated into PM₁₀ estimation to prioritize air pollution management efforts.

5 Conclusions

Our empirical model based on ground station data estimated PM₁₀ concentrations with satisfactory accuracy during the burning season (January to May) in Nan Province, Thailand. The 20% error rate was acceptable for the purpose of broadening our perspective on PM₁₀ concentrations and their relationship with LULC and fire hotspots in the study area. Most problematic PM₁₀ concentrations and fire hotspots were associated with agricultural land, disturbed forest, and dense forest areas. Locations with repeated occurrences from 2015 to 2019 showed especially strong correlations with agricultural land and forests.

As local agencies in Thailand and other developing countries face budgetary and staffing limitations, defining the most-affected areas using this method enables focusing attention and resources to the greatest possible effect. For example, agricultural and natural resources offices can use such results (locations of high air pollution density or high-frequency hotspots) for controlling or mitigating open-burning activities on agricultural land and monitoring potential forest fires. Moreover, pollution control, disaster prevention and mitigation, and public health offices can better cooperate with local villagers and farmers to properly adapt and respond to these issues.

The algorithm for PM₁₀ or AOT estimation presented here could be improved by (1) increasing/updating the number of high-quality samples, more cloud-free images with medium to high spatial resolution from various observation sensors (Park et al. 2019), PM₁₀ measurements from ground stations or reliable handheld instruments to obtain a more reliable correlation analysis (e.g., well-distributed sites with frequent records in the study area), and incorporating other covariates such as weather and climate (increased local observation source/data) that influence the amounts and patterns of PM₁₀ concentration and distribution in a study; (2) testing various types of regression algorithms or ensemble models that are applicable to the local or provincial scale (Shtein et al. 2020; Zhang et al. 2019; Zou et al. 2016a); (3) investigating other methods for aerosol retrieval or atmospheric correction using Landsat data or data with higher spatial resolution (Diao et al. 2019); and (4) considering other air pollutants that are derived from biomass burning such as SO₂ and NO₂ (Qiao et al. 2019).

The low temporal resolution of Landsat 8 results in satisfactory mapping of LULC types and PM₁₀ concentrations at local to regional levels, but it limits our ability to observe and predict the pattern and direction of PM₁₀ dispersion in near real time. Although higher-temporal-resolution products (such as those from MODIS) have better capabilities for near-real-time air quality prediction at national to global levels, they also have poorer spatial resolutions that are not suitable for identifying LULC types.

Acknowledgements This research was funded by the Faculty of Liberal Arts, Thammasat University, Thailand, grant number 3/2559. We are grateful for the data provided by the US Geological Survey (USGS); the Fire Information for Resource Management System (FIRMS), NASA; the Pollution Control Department and the Department of National Parks, Wildlife and Plant Conservation, Ministry of Natural Resources and Environment, and the Ministry of Interior, Thailand.

References

- Abdullah, S., Ismail, M., Ahmed, A. N., & Abdullah, A. M. (2019). Forecasting particulate matter concentration using linear and non-linear approaches for air quality decision support. *Atmosphere*, 10(11), 667. <https://doi.org/10.3390/atmos10110667>.






- Air Quality and Noise Management Bureau, Pollution Control Department, Ministry of Natural Resources and Environment of Thailand. (2013). Thailand's air quality information. http://air4thai.pcd.go.th/webV2/aiqi_info.php. Accessed November 20, 2017
- Benas, N., Beloconi, A., & Chrysoulakis, N. (2013). Estimation of urban PM₁₀ concentration, based on MODIS and MERIS/AATSR synergistic observations. *Atmospheric Environment*, 79, 448–454. <https://doi.org/10.1016/j.atmosenv.2013.07.012>.
- Bhaskaran, S., Phillip, N., Rahman, A., & Mallick, J. (2011). Applications of satellite data for Aerosol Optical Depth (AOD) retrievals and validation with AERONET data. *Atmospheric and Climate Sciences*, 1, 61–67. <https://doi.org/10.4236/acs.2011.12007>.
- Chu, Y., Liu, Y., Li, X., Liu, Z., Lu, H., Lu, Y., et al. (2016). A review on predicting ground PM_{2.5} concentration using satellite aerosol optical depth. *Atmosphere*, 7(10), 129. <https://doi.org/10.3390/atmos7100129>.
- Diao, M., Holloway, T., Choi, S., O'Neill, S. M., Al-Hamdan, M. Z., van Donkelaar, A., et al. (2019). Methods, availability, and applications of PM_{2.5} exposure estimates derived from ground measurements, satellite, and atmospheric models. *Journal of the Air & Waste Management*, 69(12), 1391–1414. <https://doi.org/10.1080/10962247.2019.1668498>.
- Dumitrache, R. C., Iriza, A., Maco, B. A., Barbu, C. D., Hirtl, M., Mantovani, S., et al. (2016). Study on the influence of ground and satellite observations on the numerical air-quality for PM₁₀ over Romanian territory. *Atmospheric Environment*, 143, 278–289. <https://doi.org/10.1016/j.atmosenv.2016.08.063>.
- Exelis Visual Information Solutions, Inc. (2013). ENVI Classic Tutorial: Atmospherically Correcting Hyperspectral Data Using FLAASH®. Available online: http://www.harrisgeospatial.com/portals/0/pdfs/envi/FLAASH_Hyperspectral.pdf. Accessed May 13, 2017.
- Fernández-Pacheco, V. M., López-Sánchez, C. A., Álvarez-Álvarez, E., Suárez López, M. J., García-Expósito, L., Antuña Yudego, E., et al. (2018). Estimation of PM₁₀ distribution using Landsat5 and Landsat8 remote sensing. *Proceedings*, 2(23), 1430. <https://doi.org/10.3390/proceedings2231430>.
- Glantz, P., & Tesche, M. (2012). Assessment of two aerosol optical thickness retrieval algorithms applied to MODIS Aqua and Terra measurements in Europe. *Atmospheric Measurement Techniques*, 5, 1727–1740. <https://doi.org/10.5194/amt-5-1727-2012>.
- Guo, Y., Tang, Q., Gong, D. Y., & Zhang, Z. (2017). Estimating ground-level PM_{2.5} concentrations in Beijing using a satellite-based geographically and temporally weighted regression model. *Remote Sensing of Environment*, 198, 140–149. <https://doi.org/10.1016/j.rse.2017.06.001>.
- Hadjimitsis, D. G. (2009). Aerosol optical thickness (AOT) retrieval over land using satellite image based algorithm. *Air Quality, Atmosphere and Health*, 2, 89–97. <https://doi.org/10.1007/s11869-009-0036-0>.
- Hagolle, O., Huc, M., Villa Pascual, D., & Dedieu, G. (2015). A multi-temporal and multi-spectral method to estimate aerosol optical thickness over land, for the atmospheric correction of FormoSat-2, Landsat, VENµS and Sentinel-2 Images. *Remote Sensing*, 7, 2668–2691. <https://doi.org/10.3390/rs70302668>.
- Jeensorn, T., Apichartwiwat, P., & Jinsart, W. (2018). PM₁₀ and PM_{2.5} from haze smog and visibility effect in Chiang Mai Province Thailand. *Applied Environmental Research*, 40(3), 1–10.
- Jiang, M., Sun, W., Yang, G., & Zhang, D. (2017). Modelling seasonal GWR of daily PM_{2.5} with proper auxiliary variables for the Yangtze River Delta. *Remote Sensing*, 9(4), 346. <https://doi.org/10.3390/rs9040346>.
- Junpen, A., Garivait, S., & Bonnet, S. (2013). Estimating emissions from forest fires in Thailand using MODIS active fire product and country specific data. *Asia-Pacific Journal of Atmospheric Sciences*, 49, 389. <https://doi.org/10.1007/s13143-013-0036-8>.
- Kamarul Zaman, N. A. F., Kanniah, K. D., & Kaskaoutis, D. G. (2017). Estimating particulate matter using satellite based aerosol optical depth and meteorological variables in Malaysia. *Atmospheric Research*, 193, 142–162. <https://doi.org/10.1016/j.atmosres.2017.04.019>.
- Kanniah, K. D., Kaskaoutis, D. G., San Lim, H., Latif, M. T., Kamarul Zaman, N. A. F., & Liew, J. N. (2016). Overview of atmospheric aerosol studies in Malaysia: Known and unknown. *Atmospheric Research*, 182, 302–318. <https://doi.org/10.1016/j.atmosres.2016.08.002>.
- Kliengchua, W., Cooper Meeyai, A., Worakhunpiset, S., & Tantrakarnapa, K. (2018). Relationships between meteorological parameters and particulate matter in Mae Hong Son Province, Thailand. *International Journal of Environmental Research and Public Health*, 15(12), 2801. <https://doi.org/10.3390/ijerph15122801>.
- Li, L., Chen, B., Zhang, Y., Zhao, Y., Xian, Y., Xu, G., et al. (2018). Retrieval of daily PM_{2.5} concentrations using nonlinear methods: A case study of the Beijing–Tianjin–Hebei Region, China. *Remote Sensing*, 10(12), 2006. <https://doi.org/10.3390/rs10122006>.
- Meng, X., Fu, Q., Ma, Z., Chen, L., Zou, B., Zhang, Y., et al. (2016). Estimating ground-level PM₁₀ in a Chinese city by combining satellite data, meteorological information and a land use regression model. *Environmental Pollution*, 208, 177–184. <https://doi.org/10.1016/j.envpol.2015.09.042>.

- Mishra, R. K., Pandey, J., Chaudhary, S. K., Khalkho, A., & Singh, V. K. (2012). Estimation of air pollution concentration over Jharia coalfield based on satellite imagery of atmospheric aerosol. *International Journal of Geomatics and Geosciences*, 2(3), 723–729.
- Nan Statistical Office. Annual Report 2015–2017. Available online: http://nan.nso.go.th/index.php?option=com_content&view=article&id=314:2017-10-12-03-58-03&catid=102&Itemid=507 (accessed on 19 July, 2019)
- NASA. (2018) Aerosol and flux networks. Available online: https://aeronet.gsfc.nasa.gov/new_web/networks.html. Accessed January 26, 2019
- Nguyen, T. N. T., Bui, H. Q., Pham, H. V., Luu, H. V., Man, C. D., Pham, H. N., et al. (2015). Particulate matter concentration mapping from MODIS satellite data: A Vietnamese case study. *Environmental Research Letters*, 10(9), 1–13. <https://doi.org/10.1088/1748-9326/10/9/095016>.
- Nguyen, T. N. T., Ta, V. C., Le, T. H., & Mantovani, S. (2014). Particulate matter concentration estimation from satellite aerosol and meteorological parameters: Data-driven approaches. In V. Huynh, D. Tran, A. Le, & S. Pham (Eds.), *Knowledge and systems engineering. Advances in intelligent systems and computing* (244th ed., pp. 351–362). Cham: Springer. https://doi.org/10.1007/978-3-319-02741-8_30.
- Othman, N., Jafri, M. Z. M., & San, L. H. (2010). Estimating particulate matter concentration over arid region using satellite remote sensing: A case study in Makkah, Saudi Arabia. *Modern Applied Science*, 11(4), 131–142. <https://doi.org/10.5539/mas.v4n1p131>.
- Park, S., Shin, M., Im, J., Song, C. K., Choi, M., Kim, J., et al. (2019). Estimation of ground-level particulate matter concentrations through the synergistic use of satellite observations and process-based models over South Korea. *Atmospheric Chemistry and Physics*, 19, 1097–1113. <https://doi.org/10.5194/acp-19-1097-2019>.
- Qiao, Z., Wu, F., Xu, X., Yang, J., & Liu, L. (2019). Mechanism of spatiotemporal air quality response to meteorological parameters: A national-scale analysis in China. *Sustainability*, 11(14), 3957.
- Remer, L. A., Kaufman, Y. J., Tanré, D., Matoo, S., Chu, D. A., Martins, J. V., et al. (2005). The MODIS aerosol algorithm, products, and validation. *Journal of the Atmospheric Sciences*. <https://doi.org/10.1175/JAS3385.1>.
- Roy, A., Jivani, A., & Parekh, B. (2017). Estimation of PM10 distribution using Landsat 7 ETM + remote sensing data. *International Journal of Advanced Remote Sensing & GIS*, 6(1), 2246–2252. <https://doi.org/10.23953/cloud.ijarsg.284>.
- Ryan, W. A., Gombojav, E., Barkhasragchaa, B., Byambaa, T., Lkhasuren, O., Amram, O., et al. (2013). An assessment of air pollution and its attributable mortality in Ulaanbaatar, Mongolia. *Air Quality, Atmosphere and Health*, 6(1), 137–150. <https://doi.org/10.1007/s11869-011-0154-3>.
- Saleh, S., & Hasan, G. (2014). Estimation of PM10 concentration using ground measurements and Landsat 8 OLI satellite image. *Journal of Geophysics & Remote Sensing*, 3, 1–6. <https://doi.org/10.4172/2169-0049.1000120>.
- Saraswat, I., Mishra, R. K., & Kumar, A. (2017). Estimation of PM10 concentration from Landsat 8 OLI satellite imagery over Delhi, India. *Remote Sensing Applications: Society and Environment*, 8, 251–257. <https://doi.org/10.1016/j.rsase.2017.10.006>.
- Shaheen, A., Kidwai, A. A., Ain, N. U., Aldabash, M., & Zeeshan, A. (2017). Estimating air particulate matter 10 using Landsat multi-temporal data and analyzing its annual temporal pattern over Gaza Strip, Palestine. *Journal of Asian Scientific Research*, 7(2), 22–38. <https://doi.org/10.18488/journal.2/2017.7.2/2.2.22.37>.
- Shtein, A., Kloog, I., Schwartz, J., Silibello, C., Michelozzi, P., Gariazzo, C., et al. (2020). Estimating daily PM₂₅ and PM₁₀ over Italy using an ensemble model. *Environmental Science and Technology*, 54(1), 120–128. <https://doi.org/10.1021/acs.est.9b04279>.
- Silva, R. A., West, J. J., Lamarque, J. F., Shindell, D. T., Collins, W. J., Dalsoren, S., et al. (2016). The effect of future ambient air pollution on human premature mortality to 2100 using output from the ACCMIP model ensemble. *Atmospheric Chemistry and Physics*, 16, 9847–9862. <https://doi.org/10.5194/acp-16-9847-2016>.
- Sun, L., Wei, J., Bilal, M., Tian, X., Jia, C., Guo, Y., et al. (2016). Aerosol optical depth retrieval over bright areas using Landsat 8 OLI images. *Remote Sensing*, 8(1), 1–14. <https://doi.org/10.3390/rs8010023>.
- Thai Meteorological Department. (2015) The Climate of Thailand. Available online: https://www.tmd.go.th/en/archive/thailand_climate.pdf (Accessed 3 March 2017).
- Themistocleous, K., Hadjimitsisa, D. G., Retalis, A., Chrysoulakisc, N. (2012) The development of air quality indices through image-retrieved AOT and PM10 measurements in Limassol Cyprus. In *Remote Sensing of Clouds and the Atmosphere XVII; and Lidar Technologies, Techniques, and Measurements for Atmospheric Remote Sensing VIII*. Proceedings of SPIE Vol. 8534 85340B-1, Edinburgh, United Kingdom, 1 November 2012. <https://doi.org/10.1117/12.974701>

- United States Environmental Protection Agency, July 1999, Guideline for Reporting of Daily Air Quality - Air Quality Index (AQI), 40 CFR Part 58, Appendix G.
- Vadrevu, K., Ohara, T., & Justice, C. (2018). Land cover, land use changes and air pollution in Asia: A synthesis. *Environmental Research Letters*, *12*(12), 1–17. <https://doi.org/10.1088/1748-9326/aa9c5d>.
- Vermote, E., Justice, C., Claverie, M., & Franch, B. (2016). Preliminary analysis of the performance of the Landsat 8/OLI land surface reflectance product. *Remote Sensing of Environment*, *185*, 46–56. <https://doi.org/10.1016/j.rse.2016.04.008>.
- von Hoyningen-Huene, W., Freitag, W. M., & Burrows, J. B. (2003). Retrieval of aerosol optical thickness over land surfaces from top-of-atmosphere radiance. *Journal Geophysical Research*, *108*, 1–20. <https://doi.org/10.1029/2001JD002018>.
- Wu, S., Mickley, L. J., Kaplan, J. O., & Jacob, D. J. (2012). Impacts of changes in land use and land cover on atmospheric chemistry and air quality over the 21st century. *Atmospheric Chemistry and Physics*, *12*, 1597–1609. <https://doi.org/10.5194/acp-12-1597-2012>.
- Yin, Q., Wang, J., Hu, M., & Wong, H. (2016). Estimation of daily PM_{2.5} concentration and its relationship with meteorological conditions in Beijing. *Journal of Environmental Science*, *48*, 161–168. <https://doi.org/10.1016/j.jes.2016.03.024>.
- Yoram, J. K. (1993). Aerosol optical thickness and atmospheric path radiance. *Journal Geophysical Research*, *98*(D2), 2677–2692. <https://doi.org/10.1029/92JD02427>.
- Zahari, M. A. Z., Majid, M. R., Ho, C. S., Kurata, G., Nordin, N., & Irina, S. Z. (2016). An investigation on the relationship between land use composition and PM10 pollution in Iskandar Malaysia. *Clean Technologies and Environmental*, *18*, 2429–2439. <https://doi.org/10.1007/s10098-016-1263-3>.
- Zhang, B., Zhang, M., Kang, J., Hong, D., Xu, J., & Zhu, X. (2019). Estimation of PM_x concentrations from Landsat 8 OLI images based on a multilayer perceptron neural network. *Remote Sensing*, *11*(6), 646. <https://doi.org/10.3390/rs11060646>.
- Zou, B., Chen, J., Zhai, L., Fang, X., & Zheng, Z. (2017). Satellite based mapping of ground PM_{2.5} concentration using generalized additive modeling. *Remote Sensing*, *9*(1), 1. <https://doi.org/10.3390/rs9010001>.
- Zou, B., Pu, Q., Bilal, M., Weng, Q., Zhai, L., & Nichol, J. E. (2016a). High-resolution satellite mapping of fine particulates based on geographically weighted regression. *IEEE Geoscience and Remote Sensing Letters*, *13*(4), 495–499. <https://doi.org/10.1109/LGRS.2016.2520480>.
- Zou, B., Xu, S., Sternberg, T., & Fang, X. (2016b). Effect of land use and cover change on air quality in urban sprawl. *Sustainability*, *8*(7), 677. <https://doi.org/10.3390/su8070677>.

Publisher's Note Springer Nature remains neutral with regard to jurisdictional claims in published maps and institutional affiliations.

Affiliations

Daroonwan Kamthonkiat¹  · Juthasinee Thanyapraneedkul¹  ·
Nithima Nuengjumngong¹  · Sarawut Ninsawat²  · Kessinee Unapumnu³  ·
Tuong Thuy Vu⁴ 

Juthasinee Thanyapraneedkul
yok_japan@yahoo.com

Nithima Nuengjumngong
nithima.nn@gmail.com

Sarawut Ninsawat
sarawutn@ait.ac.th

Kessinee Unapumnuk
por.kessinee@gmail.com

Tuong Thuy Vu
tuongthuy.vu@gmail.com

- ¹ Thammasat University, Klong Luang, Pathumthani 12120, Thailand
- ² Asian Institute of Technology, Klong Luang, Pathumthani 12120, Thailand
- ³ Pollution Control Department, Ministry of Natural Resources and Environment, Phahonyothin Rd, Khwaeng Samsen Nai, Khet Phaya Thai, Bangkok 10400, Thailand
- ⁴ Curtin University Malaysia, CDT 250, 98009 Miri Sarawak, Malaysia